GEOLOGY | THE GEOLOGICAL SOCIETY OF AMERICA®

https://doi.org/10.1130/G49911.1

Manuscript received 26 August 2021
Revised manuscript received 30 November 2002
Manuscript accepted 3 January 2022

Published online 8 March 2022

Millennial pulses of ore formation and an extra-high Tibetan Plateau

Yang Li[1]*, Mark B. Allen[2] and Xian-Hua Li[1]

[1]State Key Laboratory of Lithospheric Evolution, Institute of Geology and Geophysics, Chinese Academy of Sciences, Beijing 100029, China

[2]Department of Earth Sciences, Durham University, Durham DH13LE, UK

ABSTRACT

Quantifying the rhythms and rates of magmatic-hydrothermal systems is critical for a better understanding of their controls on ore formation and the dynamics of magmatic reservoirs that feed them. We reconstructed the evolution of ore-forming fluids using hydrothermal quartz from the 17.4 Ma Zhibula skarn, Tibet. Ion probe analysis reveals sharp and dramatic changes in quartz $\delta^{18}O$ values between 5‰ and –9.3‰, with fluid $\delta^{18}O$ values varying between 2.8‰ and –18.2‰, which are best explained by transient meteoric water incursion into a hydrothermal system dominated by magmatic fluids. Two pulses of magmatic fluids and a meteoric water incursion event are inferred, which operated at the millennium scale (760–1510 yr) as constrained by the aluminum diffusion chronometer. Our results indicate that magmatic reservoirs are likely water unsaturated for most of their lifetime (>10^5–10^6 yr), with transient and episodic fluid exsolutions (~10^3 yr) being driven by magma replenishment or crystallization-induced water saturation. With focused and efficient metal deposition, multiple pulses of metalliferous fluids favor the formation of giant deposits with high grade. Meteoric water $\delta^{18}O$ values (–25.4 ± 2.3‰) derived from Zhibula quartz further suggest a paleo-elevation of 5.9 ± 0.3 km; this transient early Miocene surface uplift plausibly was due to break-off of the oceanic slab attached to the Indian Plate. Our research highlights that ubiquitous hydrothermal quartz in orogenic belts can probe the dynamics of magmatic-hydrothermal systems and also quantify paleo-elevations, which has significant tectonic implications.

INTRODUCTION

The rhythms and rates of magmatic-hydrothermal and volcanic systems are the primary parameters required for a quantitative understanding of how volcanic igneous plumbing systems control ore formation and volcanism, but currently they are not well-constrained. Magmatic reservoirs at upper crustal levels (~10 km) feeding these systems are long-lived (>10^5–10^6 yr) and involve many repeated magma recharging events (Karakas et al., 2017). Therefore, hydrothermal systems are expected to be long-lived. However, recent advances in high-precision dating, numerical simulation, and diffusion modeling mostly argue for short-lived (<10^5 yr) timescales for hydrothermal systems (Weis et al., 2012; Buret et al., 2016; Cernuschi et al., 2018; Li et al., 2018). Evolution of the hydrothermal systems has a sensitive response to the dynamics of deeply seated magmatic reservoirs and determines the rates of heat loss and fluid exsolution. Upon ascent, magmatic fluids will cool and interact with meteoric water and wall rocks, then generate hydrothermal alteration assemblages and mineralization. Porphyry and skarn deposits, as an archive of ancient magmatic-hydrothermal systems, thus have the potential to tackle fluid evolution at shallow levels and probe dynamics of magmatic reservoirs at depth.

The ubiquitous interplay between magmatic fluids and meteoric water controls, and is recorded by, elemental and isotopic compositions of robust hydrothermal minerals such as quartz. Using high spatial resolution techniques such as secondary ion mass spectrometry (SIMS), which essentially translate texture-controlled information to temporal patterns, enables us to reconstruct the evolution of ore-forming fluids with unprecedented detail (Fekete et al., 2016; Rottier et al., 2021). Meteoric water oxygen isotope compositions ($\delta^{18}O_m$) are negatively correlated with paleo-elevations (Rowley and Garzione, 2007); this opens the possibility of using hydrothermal quartz to predict paleo-elevations. Additionally, robust paleo-elevations of ancient plateaus also can help understand underlying tectonics, which control surface uplift and subsidence.

We studied hydrothermal quartz from the 17.4 Ma Zhibula skarn in southern Tibet, which recorded meteoric water incursion into a magmatic fluid-dominated hydrothermal system to quantify the pulses and timescales of ore formation and then predict paleo-elevations and discuss tectonic implications.

SAMPLES AND RESULTS

We collected three samples from Zhibula drill cores (current elevation of ~5260 m; Fig. 1A), which are from the retrograde stage of skarn formation and have a close association with Cu-Mo mineralization (Figs. 1B and 1C). Molybdenite enclosed by quartz gave a Re-Os age of 17.4 ± 0.1 Ma (see Table S1 in the Supplemental Material[1]). Representative quartz grains (4.2−12.7 mm, $n = 4$) were cut into two halves along their C-axis, with petrographic (Figs. 2A and 2B) and geochemical analysis (Figs. 2G, 3A, and 3B) conducted on the first halves to mirror fluid inclusion data (Figs. 2D–2F) from the second halves.

All quartz grains are euhedral (Fig. 2A; Fig. S1) and show a four-stage growth history (Fig. 2C). Stages 1 and 2 quartz have flat and sharp terminations, respectively; stage 3 quartz is characterized by dissolution (Fig. 2A); stage 4 quartz terminates sharply.

Primary fluid inclusion assemblages (FIAs) from stage 1 mainly are rich in liquid with the

*E-mail: geoliy@outlook.com

[1]Supplemental Material. Sample information, methods and data. Please visit https://doi.org/10.1130/GEOL.S.19175903 to access the supplemental material, and contact editing@geosociety.org with any questions.

CITATION: Li, Y., Allen, M.B., and Li, X.-H., 2022, Millennial pulses of ore formation and an extra-high Tibetan Plateau: Geology, v. 50, p. 665–669, https://doi.org/10.1130/G49911.1

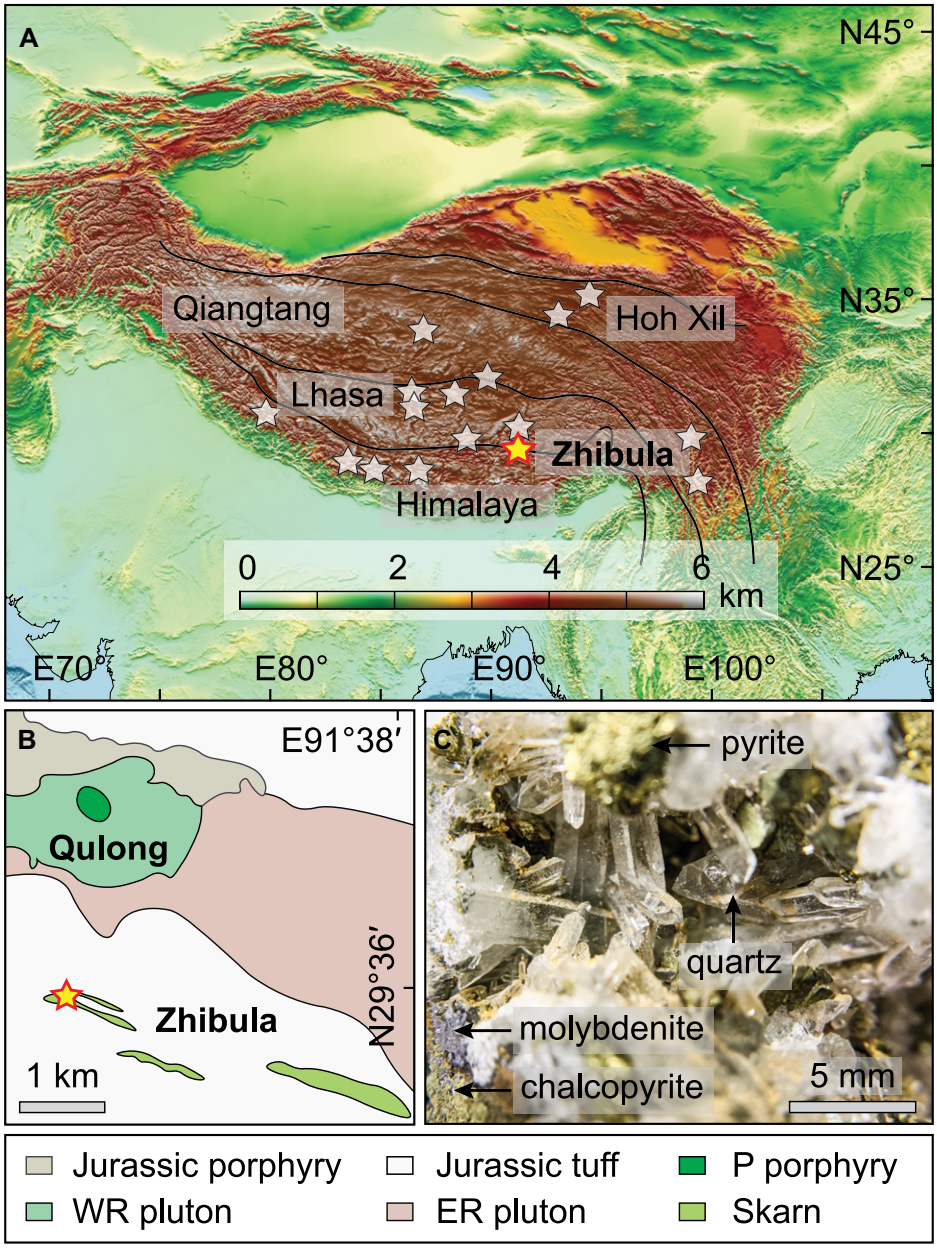

Figure 1. (A) Topographic map showing the Tibetan Plateau and adjacent regions based on the ETOPO1 Global Relief Model (https://www.ngdc.noaa.gov/mgg/global/). Stars correspond to the sampling sites of existing paleo-elevation studies (Liu et al., 2016, and references therein; Ingalls et al., 2017; Su et al., 2019). (B) Simplified geological map of the Miocene Qulong-Zhibula porphyry system, southern Tibet. Yellow star shows the location of samples from Zhibula. (C) A representative quartz-bearing sample. WR—West Rongmucuola pluton; ER—East Rongmucuola pluton; P—porphyry.

presence of halite-bearing FIAs (Fig. 2F). FIAs of stages 2–4 are rich in liquid (Figs. 2D and 2E). Homogenization temperatures (T_h, Table S2) of FIAs from stages 1, 2, and 3 are 498 ± 23 °C (2 standard deviations [SD] if not specified), 317 ± 51 °C, and 238 ± 10 °C, respectively. The T_h of stage 4 FIAs shows a rimward decrease, and FIAs from the inner zone have a T_h of 493 ± 14 °C. Brine- and halite-bearing FIAs (Fig. 2F) from stage 1 are likely to represent boiling assemblages with a trapping pressure of ~500 bars, corresponding to ~1.9 km lithostatic pressure. Trapping temperatures (T_t) for FIAs from all stages are 4–11 °C higher than those of T_h (Table S2).

All quartz grains show pronounced fluctuations in quartz $\delta^{18}O$ values. As represented by grain ZBL10 (Fig. 2G), $\delta^{18}O$ values of stage 1 quartz are stable (2.8–5.0‰), drop sharply to −3.1‰ (stage 2) before reaching a nadir of −9.3‰ (stage 3), and then rebound to a peak of 5.6‰ before finally dropping to −2.3‰ (stage 4). Corresponding fluid $\delta^{18}O$ values (Fig. 2H) calculated at T_t also show dramatic changes from 0.7‰ (stage 1), to −8.7‰ (stage 2), to −17.5‰ (stage 3), and to 2.8‰ and −5.0‰ (stage 4).

Aluminum diffusion in quartz is extremely slow (Tailby et al., 2018) and can only be resolved at ultra-high spatial resolution (i.e., 0.1 μm was used here). We selected isolated bands (Figs. 3A and 3B) to avoid potential interferences from neighboring bands. We modeled Al profiles as an initial step function modified by diffusion (Figs. 3C and 3D). Assuming a linear cooling history at 0.001 °C/yr (Li et al., 2017a), timescales at T_t (~500 °C) are 760 yr and 1510 yr for profiles a and b, respectively; using an isothermal cooling scenario, identical timescales are yielded (Figs. 3E and 3F).

The binary mixing model (Li et al., 2021, their figure 4F) allows us to calculate $\delta^{18}O_m$ values, and we obtained a maximum $\delta^{18}O_m$ value of −25.4 ± 2.3‰ at Zhibula, which corresponds to a minimum paleo-elevation of 5.9 ± 0.3 km following Rowley and Garzione (2007).

DISCUSSION

Episodic Ore-Formation Inferred from Quartz Oxygen Isotope Fluctuations

With primary magmatic fluids having a $\delta^{18}O$ value of 7.6 ± 0.5‰ (Li et al., 2018), and wall rocks (igneous rocks and carbonates) having higher $\delta^{18}O$ values, low fluid $\delta^{18}O$ values ($\delta^{18}O_f$, between 2.8‰ and −17.5‰; Fig. 2H) require incursion of meteoric water. The high temperatures (~500 °C) and salinities (Fig. 2F) of stage 1 fluids reflect magmatic affinity. The dramatic drop in temperatures (~350 °C and ~250 °C) and $\delta^{18}O_f$ values (−8.7‰ and −18.2‰) in stages 2 and 3 indicates a sudden meteoric water incursion into a magmatic-hydrothermal system originally dominated by magmatic fluids. Cooling induced by fluid mixing is an important and efficient deposition mechanism (Shu et al., 2020); it also causes quartz undersaturation (Rusk and Reed, 2002) and provides space for metal deposition, as supported by the dissolution texture in stage 3 quartz (Fig. 2A). The sharp rebound of temperature (>494 °C) and $\delta^{18}O_f$ values (2.8‰) at the beginning of stage 4 is best explained by further pulses of magmatic fluids, which are likely accompanied by the emplacement of syn-ore intrusions.

As such, at least two pulses of magmatic fluid replenishment and one meteoric water incursion event occurred during skarn formation at Zhibula. This does not exclude the plausible presence of more pulses. This cyclical process is very common for many magmatic-hydrothermal systems (D'Errico et al., 2012; Li et al., 2018). Release of metalliferous fluids will bring appreciable amounts of metals to the shallow levels; with efficient and focused deposition, the presence of multiple pulses will favor the formation of giant deposits with high grade.

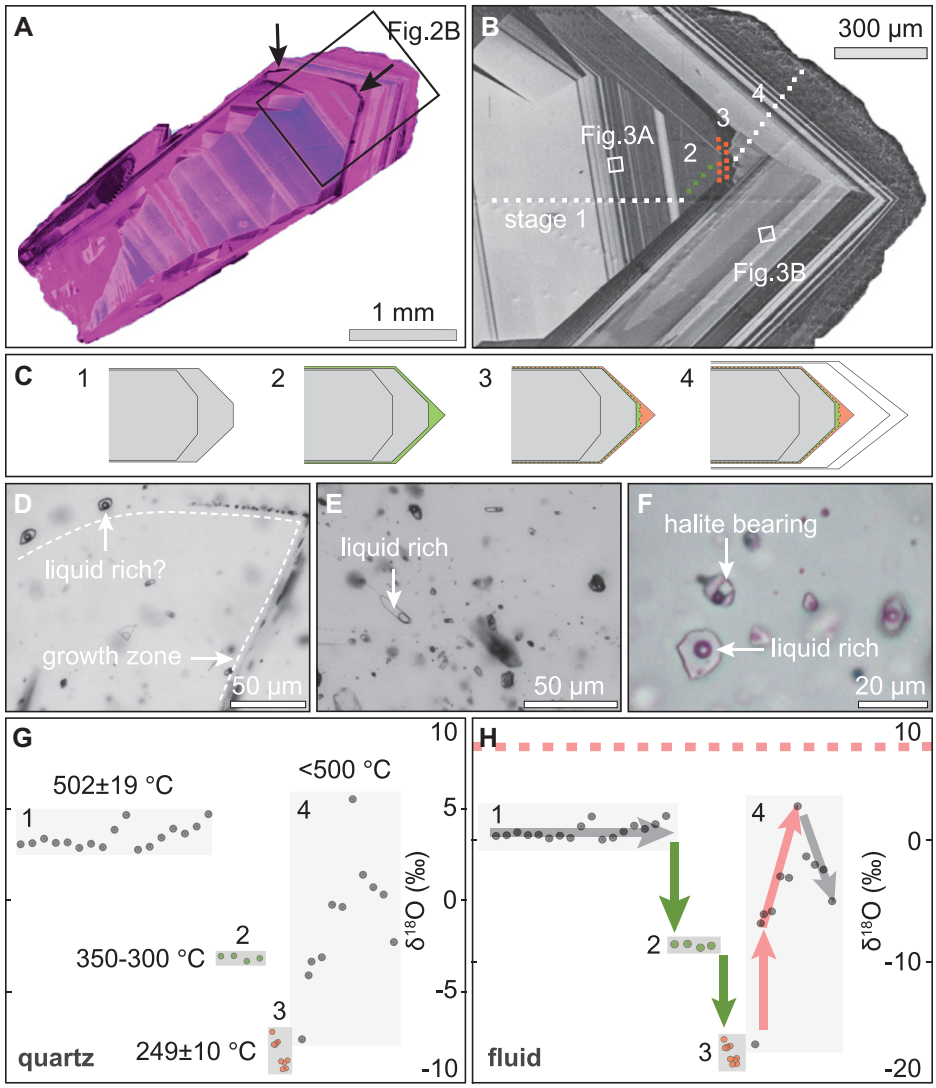

Figure 2. (A) False color cathodoluminescence (CL) image of a representative quartz crystal from the Zhibula skarn, Tibet. Arrows highlight the dissolution textures from stage 3 of quartz growth history. (B) Transects (white, green, and orange squares) on a CL image showing secondary ion mass spectrometry (SIMS) spots for quartz $\delta^{18}O$ analysis. Also shown are two areas imaged by nanoscale secondary ion mass spectrometry (NanoSIMS) for Al diffusion chronometry. (C) The four-stage growth history inferred from petrographic observations. Stages 1 and 2 quartz bear flat and sharp terminates, respectively; stage 3 quartz is characterized by a dissolution-reprecipitation texture, and stage 4 quartz terminates sharply. (D) Primary fluid inclusions (FIAs) along growth zones from stage 4 are rich in liquid. (E) Liquid-rich FIAs from stage 2. (F) Liquid-rich and halite-bearing FIAs from stage 1 form boiling assemblages. (G) SIMS $\delta^{18}O$ values of Zhibula quartz. Trapping temperatures (T_t) of FIAs also are shown. (H) Calculated $\delta^{18}O$ values of ore-forming fluids at T_t. Gray, green, and orange dots indicate fluid $\delta^{18}O$ values calculated from quartz $\delta^{18}O$ values. Dashed, pink line represents $\delta^{18}O$ values of primary magmatic fluids (7.6 ± 0.5‰; Li et al., 2018). Stage 1 quartz was precipitated from high-temperature fluids with a magmatic affinity. Significantly meteoric water incursion in stages 2 and 3 led to dramatic drops in temperature and $\delta^{18}O_f$ (f—fluid) values, and cooling-induced quartz unsaturation also caused dissolution. Rebound of temperature and $\delta^{18}O_f$ values at the beginning of stage 4 recorded recharge of magmatic fluids; further cooling and potential meteoric water incursion were inferred as well. Very depleted $\delta^{18}O$ values of meteoric water recorded by stages 2 and 3 quartz permit the application of paleo-altimetry.

Millennial Hydrothermal Pulses Constrained by Aluminum Diffusion in Quartz

Our Al diffusion in quartz suggests that episodic hydrothermal pulses likely operated on the millennium scale (760−1510 yr; Figs. 3E and 3F) at ~500 °C. The diffusion clock may have been reset with the presence of multiple magmatic-hydrothermal pulses; if more pulses were present, then our timescales represent cumulative averages and are overestimated. Magmatic reservoirs feeding the volcanic igneous plumbing systems are stored in a high-crystallinity state near-solidus (>50% crystals) for most of their lifetime (>10^5−10^6 yr) (Karakas et al., 2017; Rubin et al., 2017; Jackson et al., 2018), with rapid thermal rejuvenation (<10^5 yr) being generated by multiple small intrusions (Buret et al., 2016; Tapster et al., 2016; Szymanowski et al., 2017). For example, during the 4.4 × 10^5 yr of magma evolution at Fish Canyon (Colorado, USA), the recharge of andesitic magma into a reservoir with high crystallinity was responsible for generating ~5000 km^3 of erupted dacite (Wotzlaw et al., 2013). To reconcile the contrasting timescales of hydrothermal systems and the magmatic reservoirs feeding them, we hypothesize that magmatic reservoirs spend most of their time in water-unsaturated conditions, and only become water-saturated transiently when the reservoir transforms from a "cold" to "hot" state upon magma replenishment (Cooper and Kent, 2014). Indeed, temporal evolution of magmatic volatiles at Campi Flegrei, Italy, suggests that the underlying magma reservoir remained persistently water-undersaturated throughout most of its lifetime and only reached saturation just before eruption (Stock et al., 2016).

To summarize, we argue that fluid exsolution likely operates transiently during the prolonged lifetime (>10^5−10^6 yr) of magma reservoirs, with episodic magma replenishment on millennium timescales being the most important driving force to punctuate the stabilities of magma reservoirs. Second boiling [volatile-saturated melts → crystals + volatiles (H_2O, Cl, S)], following extensive magma crystallization, is also a way to bridge the gap between long magma evolution and rapid ore formation. In this process, volatile accommodation generates overpressure in the deep-seated magmatic reservoir, and the release of hot fluids is accompanied by decompression, with mechanical energy being released efficiently (Burnham, 1985). Cyclical pressure changes and energy releases in turn fracture wall rocks, facilitate accelerated magma crystallization, and promote more efficient and episodic metalliferous fluid expulsion (Norton, 1984). Currently, we are unable to decipher the exact trigger (e.g., recharge vs. crystallization) that controls this rapid and cyclical pattern of fluid evolution, and further petrological and modeling work is needed.

An Extra-High Tibetan Plateau and Tectonic Implications

Using our binary mixing model (Li et al., 2021), the $\delta^{18}O_m$ values recorded by Zhibula quartz are −25.4 ± 2.3‰, corresponding to a paleo-elevation of 5.9 ± 0.3 km (Fig. 4D; Table S6). The sensitivity of calculated paleo-elevation on input parameters is insignificant, and changes in paleo-elevations are <400 m even in extreme scenarios (Fig. S3). Oxygen isotope–based altimetry requires the application of Rayleigh distillation in deep time (Botsyun et al., 2019), and our study site is located in a

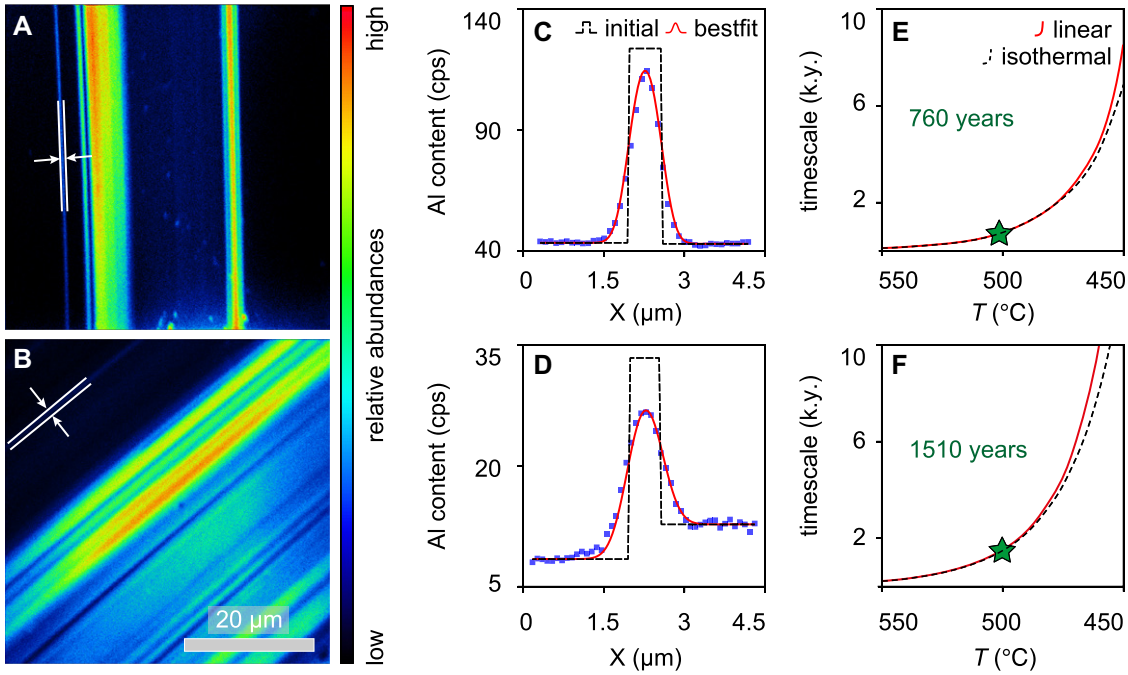

Figure 3. (A,B) Nanoscale secondary ion mass spectrometry (NanoSIMS) aluminum mapping of stages 1 (A) and 4 (B) (growth history) quartz, as shown in Figure 2A. Arrows highlight the bands selected for diffusion chronometer study. (C,D) Aluminum profiles at the concentration boundary (highlighted by arrows in Figs. 3A and 3B) are shown as blue rectangles; the initial step functions for modeling are shown by the dashed black lines, and the best modeled diffusion profiles are shown as red lines. The diffusional profiles are ~1.2 μm in length, and resolving diffusion at such a fine scale requires analytical techniques with an ultrahigh spatial resolution (e.g., 0.1 μm used here); to avoid potential interference from neighboring bands, only isolated bands are targeted for diffusion modeling. (E,F) Best-fit diffusion time of Al in quartz as a function of temperature, with diffusion time computed following a cooling rate of 0.001 °C/yr (Li et al., 2017a), and an isothermal cooling scenario (red solid and dashed black lines, respectively). The green stars represent timescales at quartz formation temperatures constrained by fluid inclusion studies.

region appropriate for such a purpose (Shen and Poulsen, 2019). These paleo-elevation values at 17.4 Ma are slightly higher (0.9 ± 0.3 km) than the current average elevation of the Tibetan Plateau at ~5 km (Figs. 4A–4D). Additionally, our fluid inclusion data indicate a paleo-depth of 1.9 km for the samples studied (current depth <260 m), and this would require an erosion of 1.6 km at the Zhibula area, similar to our previous fluid inclusion study (Li et al., 2017b), which also argues for a higher-than-present paleo-elevation.

The existence of an extra-high elevation in southern Tibet before extension is consistent with break-off of the oceanic slab at the leading edge of the Indian Plate by the early Miocene (Magni et al., 2017). Scenarios for active tectonics, where extension occurs during insertion or underthrusting of the Indian Plate without net subsidence (Kapp and Guynn, 2004; Styron et al., 2015), did not apply at the onset of rifting. We propose that rapid surface uplift by ca. 20 Ma followed initial slab break-off and produced the peak elevations recorded in southern Tibet by the Zhibula hydrothermal system (Fig. 4E). This timing is similar to early activity of the South Tibetan Detachment System within the Himalaya (Kellett et al., 2010) and supports models for early Miocene slab break-off, which is among the plethora of suggested ages for this tectonic event (Garzanti et al., 2018). Subsequent rotation and underplating of the Indian Plate reduced the amount of rock uplift (Magni et al., 2017) and was followed by northward underthrusting that has continued to present (Fig. 4F).

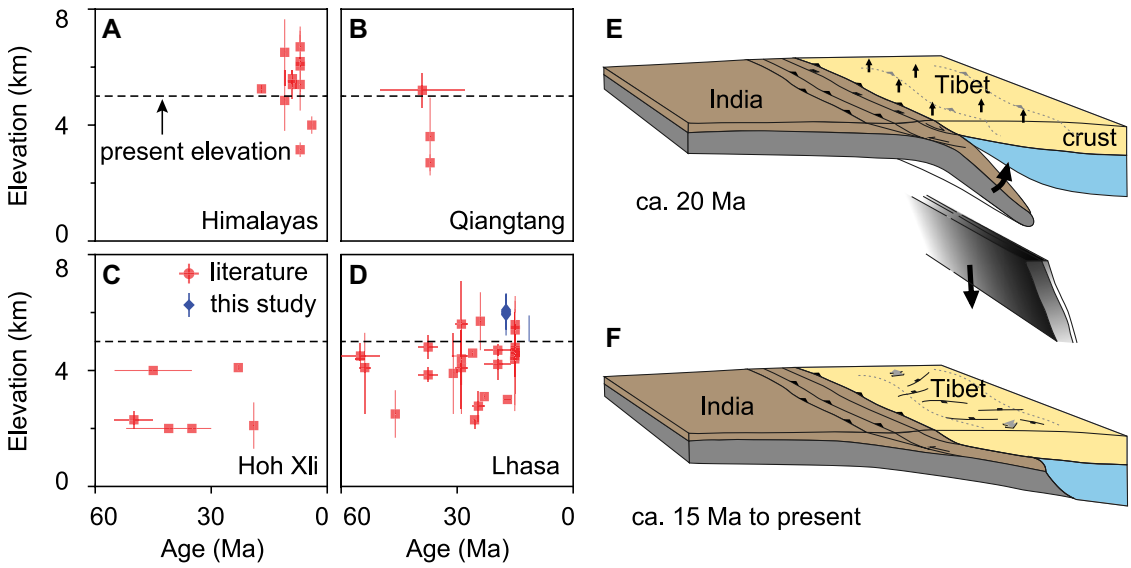

Figure 4. (A–D) Paleo-elevations of the Tibetan Plateau by region. Data from Zhibula skarn hydrothermal quartz are comparable to but slightly higher than data from the literature (Liu et al., 2016, and references therein; Ingalls et al., 2017; Su et al., 2019). See Figure 1 for locations. (E) Initial slab break-off causes peak rock uplift in southern Tibet and extra-high plateau elevation by ca. 20 Ma. (F) Underthrusting of the Indian Plate beneath southern Tibet accompanies rifting and subsidence of the southern Tibetan Plateau from ca. 15 Ma to the present. Uncertainties are plotted at the 2σ level.

The existence of an extra-high Tibetan Plateau in the early Miocene also has implications for climatic evolution because the plateau drives the South and East Asian monsoon systems through a combination of thermal and mechanical forcing, with high topography forming a barrier to southward and northward air flow (Molnar et al., 2010).

ACKNOWLEDGMENTS

This study is funded by the National Key Research and Development Program of China (grant 2018YFA0702600), the National Natural Science Foundation of China (grant 42022022), and the Pioneer Hundred Talents Program of the Chinese Academy of Sciences. We thank Urs Schaltegger for editorial handling. The paper benefitted significantly from the constructive comments of the reviewers.

REFERENCES CITED

Botsyun, S., Sepulchre, P., Donnadieu, Y., Risi, C., Licht, A., and Caves Rugenstein, J.K., 2019, Revised paleoaltimetry data show low Tibetan Plateau elevation during the Eocene: Science, v. 363, eaaq1436, https://doi.org/10.1126/science.aaq1436.

Buret, Y., von Quadt, A., Heinrich, C., Selby, D., Walle, M., and Peytcheva, I., 2016, From a long-lived upper-crustal magma chamber to rapid porphyry copper-emplacement: Reading the geochemistry of zircon crystals at Bajo de la Alumbrera (NW Argentina): Earth and Planetary Science Letters, v. 450, p. 120–131, https://doi.org/10.1016/j.epsl.2016.06.017.

Burnham, C.W., 1985, Energy release in subvolcanic environments; implications for breccia formation: Economic Geology, v. 80, p. 1515–1522, https://doi.org/10.2113/gsecongeo.80.6.1515.

Cernuschi, F., Dilles, J.H., Grocke, S.B., Valley, J.W., Kitajima, K., and Tepley, F.J., 2018, Rapid formation of porphyry copper deposits evidenced by diffusion of oxygen and titanium in quartz: Geology, v. 46, p. 611–614, https://doi.org/10.1130/G40262.1.

Cooper, K.M., and Kent, A.J., 2014, Rapid remobilization of magmatic crystals kept in cold storage: Nature, v. 506, p. 480–483, https://doi.org/10.1038/nature12991.

D'Errico, M.E., Lackey, J.S., Surpless, B.E., Loewy, S.L., Wooden, J.L., Barnes, J.D., Strickland, A., and Valley, J.W., 2012, A detailed record of shallow hydrothermal fluid flow in the Sierra Nevada magmatic arc from low-$\delta^{18}O$ skarn garnets: Geology, v. 40, p. 763–766, https://doi.org/10.1130/G33008.1.

Fekete, S., Weis, P., Driesner, T., Bouvier, A.-S., Baumgartner, L., and Heinrich, C.A., 2016, Contrasting hydrological processes of meteoric water incursion during magmatic-hydrothermal ore deposition: An oxygen isotope study by ion microprobe: Earth and Planetary Science Letters, v. 451, p. 263–271, https://doi.org/10.1016/j.epsl.2016.07.009.

Garzanti, E., Radeff, G., and Malusà, M.G., 2018, Slab breakoff: A critical appraisal of a geological theory as applied in space and time: Earth-Science Reviews, v. 177, p. 303–319, https://doi.org/10.1016/j.earscirev.2017.11.012.

Ingalls, M., et al., 2017, Paleocene to Pliocene low-latitude, high-elevation basins of southern Tibet: Implications for tectonic models of India-Asia collision, Cenozoic climate, and geochemical weathering: Geological Society of America Bulletin, v. 130, p. 307–330, https://doi.org/10.1130/B31723.1.

Jackson, M.D., Blundy, J., and Sparks, R.S.J., 2018, Chemical differentiation, cold storage and remobilization of magma in the Earth's crust: Nature, v. 564, p. 405–409, https://doi.org/10.1038/s41586-018-0746-2.

Kapp, P., and Guynn, J.H., 2004, Indian punch rifts Tibet: Geology, v. 32, p. 993–996, https://doi.org/10.1130/G20689.1.

Karakas, O., Degruyter, W., Bachmann, O., and Dufek, J., 2017, Lifetime and size of shallow magma bodies controlled by crustal-scale magmatism: Nature Geoscience, v. 10, p. 446–450, https://doi.org/10.1038/ngeo2959.

Kellett, D.A., Grujic, D., Warren, C., Cottle, J., Jamieson, R., and Tenzin, T., 2010, Metamorphic history of a syn-convergent orogen-parallel detachment: The South Tibetan detachment system, Bhutan Himalaya: Journal of Metamorphic Geology, v. 28, p. 785–808, https://doi.org/10.1111/j.1525-1314.2010.00893.x.

Li, Y., Selby, D., Condon, D., and Tapster, S., 2017a, Cyclic magmatic-hydrothermal evolution in porphyry systems: High-precision U-Pb and Re-Os geochronology constraints on the Tibetan Qulong porphyry Cu-Mo deposit: Economic Geology, v. 112, p. 1419–1440, https://doi.org/10.5382/econgeo.2017.4515.

Li, Y., Selby, D., Feely, M., Costanzo, A., and Li, X.H., 2017b, Fluid inclusion characteristics and molybdenite Re-Os geochronology of the Qulong porphyry copper-molybdenum deposit, Tibet: Mineralium Deposita, v. 52, p. 137–158, https://doi.org/10.1007/s00126-016-0654-z.

Li, Y., Li, X.-H., Selby, D., and Li, J.-W., 2018, Pulsed magmatic fluid release for the formation of porphyry deposits: Tracing fluid evolution in absolute time from the Tibetan Qulong Cu-Mo deposit: Geology, v. 46, p. 7–10, https://doi.org/10.1130/G39504.1.

Li, Y., He, S., Zhang, R.-Q., Bi, X.-W., Feng, L.-J., Tang, G.-Q., Wang, W.-Z., Huang, F., and Li, X.-H., 2021, Cassiterite oxygen isotopes in magmatic-hydrothermal systems in situ microanalysis, fractionation factor and application: Mineralium Deposita, https://doi.org/10.1007/s00126-021-01068-x.

Liu, X., Xu, Q., and Ding, L., 2016, Differential surface uplift: Cenozoic paleoelevation history of the Tibetan Plateau: Science China Earth Sciences, v. 59, p. 2105–2120, https://doi.org/10.1007/s11430-015-5486-y.

Magni, V., Allen, M.B., van Hunen, J., and Bouilhol, P., 2017, Continental underplating after slab break-off: Earth and Planetary Science Letters, v. 474, p. 59–67, https://doi.org/10.1016/j.epsl.2017.06.017.

Molnar, P., Boos, W.R., and Battisti, D.S., 2010, Orographic controls on climate and paleoclimate of Asia: Thermal and mechanical roles for the Tibetan Plateau: Annual Review of Earth and Planetary Sciences, v. 38, p. 77–102, https://doi.org/10.1146/annurev-earth-040809-152456.

Norton, D.L., 1984, Theory of hydrothermal systems: Annual Review of Earth and Planetary Sciences, v. 12, p. 155–177, https://doi.org/10.1146/annurev.ea.12.050184.001103.

Rottier, B., Kouzmanov, K., Casanova, V., Bouvier, A.-S., Baumgartner, L.P., Wälle, M., and Fontboté, L., 2021, Tracking fluid mixing in epithermal deposits—Insights from *in-situ* $\delta^{18}O$ and trace element composition of hydrothermal quartz from the giant Cerro de Pasco polymetallic deposit, Peru: Chemical Geology, v. 576, 120277, https://doi.org/10.1016/j.chemgeo.2021.120277.

Rowley, D.B., and Garzione, C.N., 2007, Stable isotope-based paleoaltimetry: Annual Review of Earth and Planetary Sciences, v. 35, p. 463–508, https://doi.org/10.1146/annurev.earth.35.031306.140155.

Rubin, A.E., Cooper, K.M., Till, C.B., Kent, A.J.R., Costa, F., Bose, M., Gravley, D., Deering, C., and Cole, J., 2017, Rapid cooling and cold storage in a silicic magma reservoir recorded in individual crystals: Science, v. 356, p. 1154–1156, https://doi.org/10.1126/science.aam8720.

Rusk, B., and Reed, M., 2002, Scanning electron microscope-cathodoluminescence analysis of quartz reveals complex growth histories in veins from the Butte porphyry copper deposit, Montana: Geology, v. 30, p. 727–730, https://doi.org/10.1130/0091-7613(2002)030<0727:SEMCAO>2.0.CO;2.

Shen, H., and Poulsen, C.J., 2019, Precipitation $\delta^{18}O$ on the Himalaya-Tibet orogeny and its relationship to surface elevation: Climate of the Past, v. 15, p. 169–187, https://doi.org/10.5194/cp-15-169-2019.

Shu, Q., Chang, Z., and Mavrogenes, J., 2020, Fluid compositions reveal fluid nature, metal deposition mechanisms, and mineralization potential: An example at the Haobugao Zn-Pb skarn, China: Geology, v. 49, p. 473–477, https://doi.org/10.1130/G48348.1.

Stock, M.J., Humphreys, M.C.S., Smith, V.C., Isaia, R., and Pyle, D.M., 2016, Late-stage volatile saturation as a potential trigger for explosive volcanic eruptions: Nature Geoscience, v. 9, p. 249–254, https://doi.org/10.1038/ngeo2639.

Styron, R., Taylor, M., and Sundell, K., 2015, Accelerated extension of Tibet linked to the northward underthrusting of Indian crust: Nature Geoscience, v. 8, p. 131, https://doi.org/10.1038/ngeo2336.

Su, T., et al., 2019, No high Tibetan Plateau until the Neogene: Science Advances, v. 5, eaav2189, https://doi.org/10.1126/sciadv.aav2189.

Szymanowski, D., Wotzlaw, J.-F., Ellis, B.S., Bachmann, O., Guillong, M., and von Quadt, A., 2017, Protracted near-solidus storage and pre-eruptive rejuvenation of large magma reservoirs: Nature Geoscience, v. 10, p. 777–782, https://doi.org/10.1038/ngeo3020.

Tailby, N.D., Cherniak, D.J., and Watson, E.B., 2018, Al diffusion in quartz: The American Mineralogist, v. 103, p. 839–847, https://doi.org/10.2138/am-2018-5613.

Tapster, S., Condon, D.J., Naden, J., Noble, S.R., Petterson, M.G., Roberts, N.M.W., Saunders, A.D., and Smith, D.J., 2016, Rapid thermal rejuvenation of high-crystallinity magma linked to porphyry copper deposit formation; Evidence from the Koloula Porphyry Prospect, Solomon Islands: Earth and Planetary Science Letters, v. 442, p. 206–217, https://doi.org/10.1016/j.epsl.2016.02.046.

Weis, P., Driesner, T., and Heinrich, C.A., 2012, Porphyry-copper ore shells form at stable pressure-temperature fronts within dynamic fluid plumes: Science, v. 338, p. 1613–1616, https://doi.org/10.1126/science.1225009.

Wotzlaw, J.-F., Schaltegger, U., Frick, D.A., Dungan, M.A., Gerdes, A., and Günther, D., 2013, Tracking the evolution of large-volume silicic magma reservoirs from assembly to supereruption: Geology, v. 41, p. 867–870, https://doi.org/10.1130/G34366.1.

Printed in USA